BSM HIGGS AND DI-HIGGS PHYSICS AT THE LHEC AND FCC-HE

Mukesh Kumar
NITHEP, MITP & School of Physics,
University of the Witwatersrand
Johannesburg, South Africa.

DIS17
April 3-7 2017, University of Birmingham

On behalf of LHeC and FCC-he Higgs-Top group

LHeC/FCC-he

A Baseline for the FCC-he

Oliver Brüning[1] Max Klein[1,2], Daniel Schulte[1], Frank Zimmermann[1]
[1] CERN, [2] University of Liverpool
March 3^{rd}, 2016

Table 1: Baseline parameters of future electron-proton collider configurations based on the ERL electron linac.

parameter [unit]	LHeC CDR	ep at HL-LHC	ep at HE-LHC	FCC-he
E_p [TeV]	7	7	15	50
E_e [GeV]	60	60	60	60
$\sqrt{s}$ [TeV]	1.3	1.3	1.9	3.5
bunch spacing [ns]	25	25	25	25
protons per bunch [10^{11}]	1.7	2.2	2.2	1
ϵ_p [μm]	3.7	2	2	2.2
electrons per bunch [10^9]	1	2.3	2.3	2.3
electron current [mA]	6.4	15	15	15
IP beta function β_p^* [cm]	10	7	10	15
hourglass factor	0.9	0.9	0.9	0.9
pinch factor	1.3	1.3	1.3	1.3
luminosity [10^{33}cm^{-2}s^{-1}]	1.3	10.1	15.1	9.2

I.

PHYSICAL REVIEW D 82, 016009 (2010)

Higgs boson searches and the $Hb\bar{b}$ coupling at the LHeC

Tao Han* and Bruce Mellado†

Department of Physics, University of Wisconsin, Madison, Wisconsin 53706, USA

(Received 15 September 2009; published 30 July 2010)

Once the existence of the Higgs boson is established at the CERN Large Hadron Collider (LHC), the focus will be shifted toward understanding its couplings to other particles. A crucial aspect is the measurement of the bottom Yukawa coupling, which is challenging at the LHC. In this paper we study the use of forward jet tagging as a means to secure the observation and to significantly improve the purity of the Higgs boson signal in the $H \to b\bar{b}$ decay mode from deep inelastic electron-proton scattering at the LHC. We demonstrate that the requirement of forward jet tagging in charged current events strongly enhances the signal-to-background ratio. The impact of a veto on additional partons is also discussed. Excellent response to hadronic shower and b-tagging capabilities are pivotal detector performance aspects.

DOI: 10.1103/PhysRevD.82.016009 PACS numbers: 11.15.Ex, 14.80.Bn

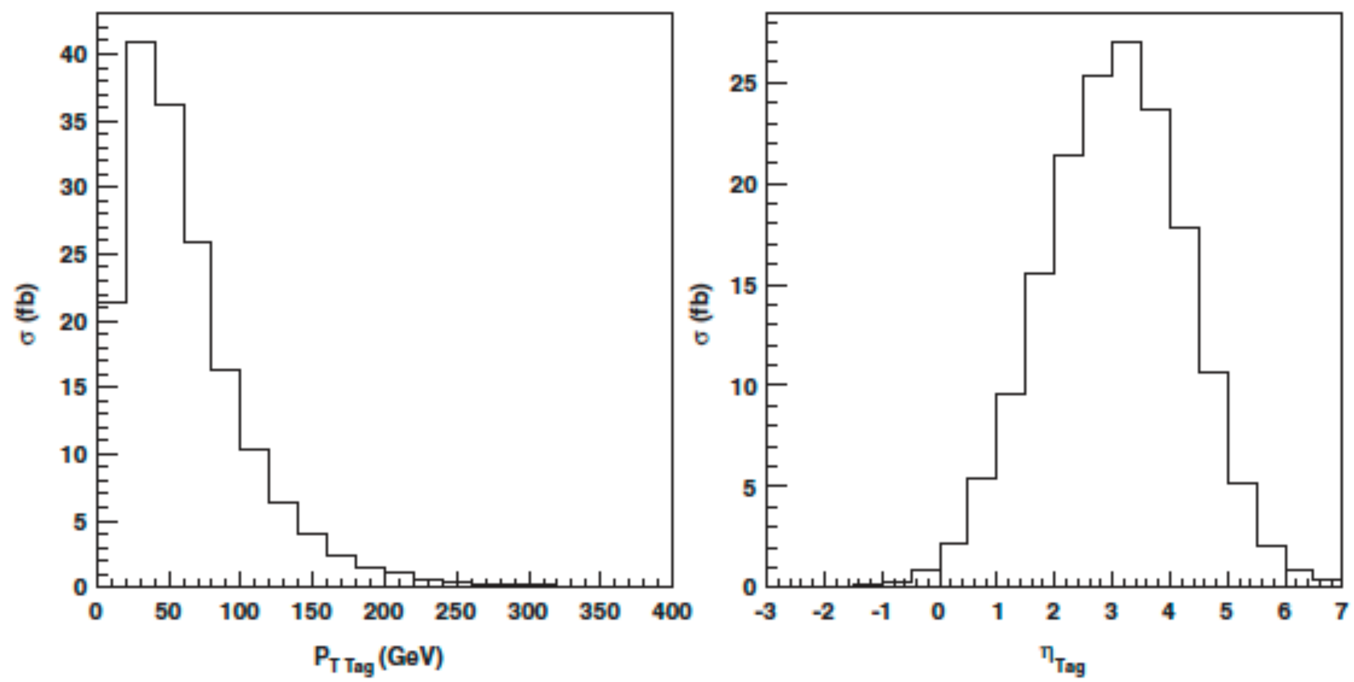

consider the physics potential for the proposed proton-electron collider, the LHeC. We studied the use of forward jet tagging as a means to secure the observation of the Higgs boson in the $H \to b\bar{b}$ decay mode, and to significantly improve the purity of the signal. An excellent signal-to-background ratio of almost a factor of 5 can be achieved for the CC process while allowing for a significant rate of Higgs boson events. With this we believe that a measurement of the bottom Yukawa coupling at the LHeC may be feasible by means of combining the knowledge from the LHC on $H \to WW^\star$, $\tau\tau$.

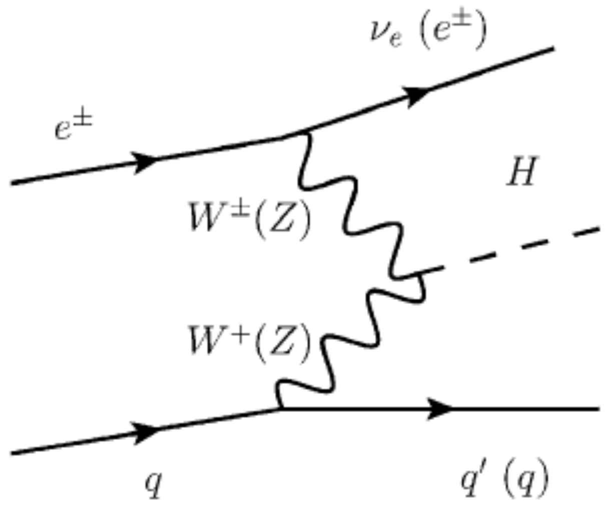

FIG. 1. Leading order diagram for the production of a standard model Higgs boson in ep collisions for the charged current and neutral current processes.

$$\sigma(fa \to f'X) \approx \int dx dp_T^2 P_{V/f}(x, p_T^2)\sigma(Va \to X)$$

$$P^T_{V/f}(x, p_T^2) = \frac{g_V^2 + g_A^2}{8\pi^2}\frac{1+(1-x)^2}{x}\frac{p_T^2}{(p_T^2 + (1-x)M_V^2)^2} \quad (4)$$

$$P^L_{V/f}(x, p_T^2) = \frac{g_V^2 + g_A^2}{4\pi^2}\frac{1-x}{x}\frac{(1-x)M_V^2}{(p_T^2 + (1-x)M_V^2)^2}. \quad (5)$$

These expressions lead us to the following observations:

(1) Unlike the QCD partons that scale like $1/p_T^2$ at the low transverse momentum, the final state quark f' typically has $p_T \sim \sqrt{1-x}M_V \leq M_W$.

(2) Because of the $1/x$ behavior for the gauge boson distribution, the outgoing parton energy $(1-x)E$ tends to be high. Consequently, it leads to an energetic forward jet with small, but finite, angle with respect to the beam.

(3) At high p_T, $P^T_{V/f} \sim 1/p_T^2$ and $P^L_{V/f} \sim 1/p_T^4$, and thus the contribution from the longitudinally polarized gauge bosons is relatively suppressed at high p_T to that of the transversely polarized.

II.

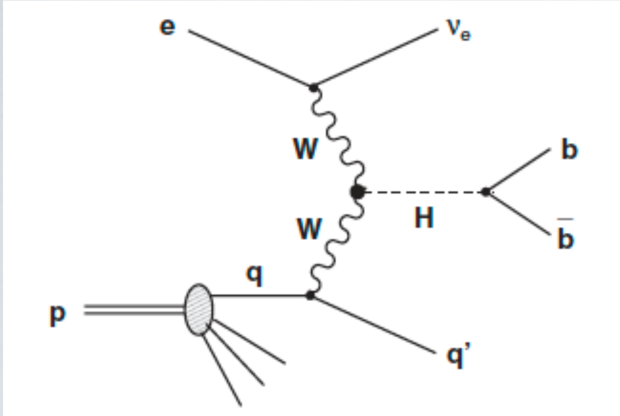

PRL 109, 261801 (2012) PHYSICAL REVIEW LETTERS

Azimuthal Angle Probe of Anomalous HWW Couplings at a High Energy ep Collider

Sudhansu S. Biswal,[1] Rohini M. Godbole,[2] Bruce Mellado,[3,4] and Sreerup Raychaudhuri[5]

$$\mathcal{L}_{\rm int} = -gM_W\left(W_\mu W^\mu + \frac{1}{2\cos\theta_W} Z_\mu Z^\mu\right)H.$$

$$\Gamma^{\rm BSM}_{\mu\nu}(p,q) = \frac{g}{M_W}[\lambda(p\cdot q g_{\mu\nu} - p_\nu q_\mu) + i\lambda'\epsilon_{\mu\nu\rho\sigma}p^\rho q^\sigma],$$

$$e^-(k_1) + q(k_2) \rightarrow \nu_e(p_1) + q'(p_2) + H(p_3)$$

$$\overline{|\mathcal{M}|^2} = \left(\frac{4\pi^3\alpha^3}{\sin^6\theta_W}\right)\frac{1}{M_W^2(\hat{t}_1 - M_W^2)^2(\hat{u}_2 - M_W^2)^2} \times [4M_W^4\hat{s}\hat{s}_1 + \lambda^2\{\hat{t}_1\hat{u}_2(\hat{s}^2 + \hat{s}_1^2 + \hat{t}_1\hat{u}_2 - 2\hat{t}_2\hat{u}_1) + (\hat{s}\hat{s}_1 - \hat{t}_2\hat{u}_1)^2\}$$
$$+ 2\lambda M_W^2(\hat{s} + \hat{s}_1)(\hat{s}\hat{s}_1 + \hat{t}_1\hat{u}_2 - \hat{t}_2\hat{u}_1) + \lambda'^2\{\hat{t}_1\hat{u}_2(\hat{s}^2 + \hat{s}_1^2 - \hat{t}_1\hat{u}_2 + 2\hat{t}_2\hat{u}_1) - (\hat{s}\hat{s}_1 - \hat{t}_2\hat{u}_1)^2\}$$
$$- 2\lambda' M_W^2(\hat{s} - \hat{s}_1)(\hat{s}\hat{s}_1 + \hat{t}_1\hat{u}_2 - \hat{t}_2\hat{u}_1) + 2\lambda\lambda'\hat{t}_1\hat{u}_2(\hat{s}_1^2 - \hat{s}^2)],$$

criteria may be summarized as follows: (1) It is required that $MET > 25$ GeV. (2) Two b partons with $p_T^b > 30$ GeV and $|\eta_b| < 2.5$ must be present. The invariant mass of these b partons must lie within 10 GeV of the Higgs boson mass. (3) Of the remaining partons, the leading one must have $p_T > 30$ GeV and $1 < \eta < 5$. This will be called the forward tagging parton. (4) We require $\Delta\varphi_{{\rm MET}-J} > 0.2$ rad for all the jets (J). (5) A veto on leptons ($\ell = e, \mu, \tau$) with $p_T^\ell > 10$ GeV and $|\eta_\ell| < 2.5$ is required. (6) The invariant mass of the Higgs boson candidate and the forward tagging jet must be greater than 250 GeV. (7) We require a b-tagging efficiency $\varepsilon_b = 0.6$ for $|\eta_b| < 2.5$. The mistagging factors for c and light quark jets are taken as 0.1 and 0.01, respectively.

$$\mathcal{M}_\lambda \propto +\lambda\vec{p}_{T1}.\vec{p}_{T2}, \qquad \mathcal{M}'_\lambda \propto -\lambda'\vec{p}_{T1}.\vec{p}_{T2},$$

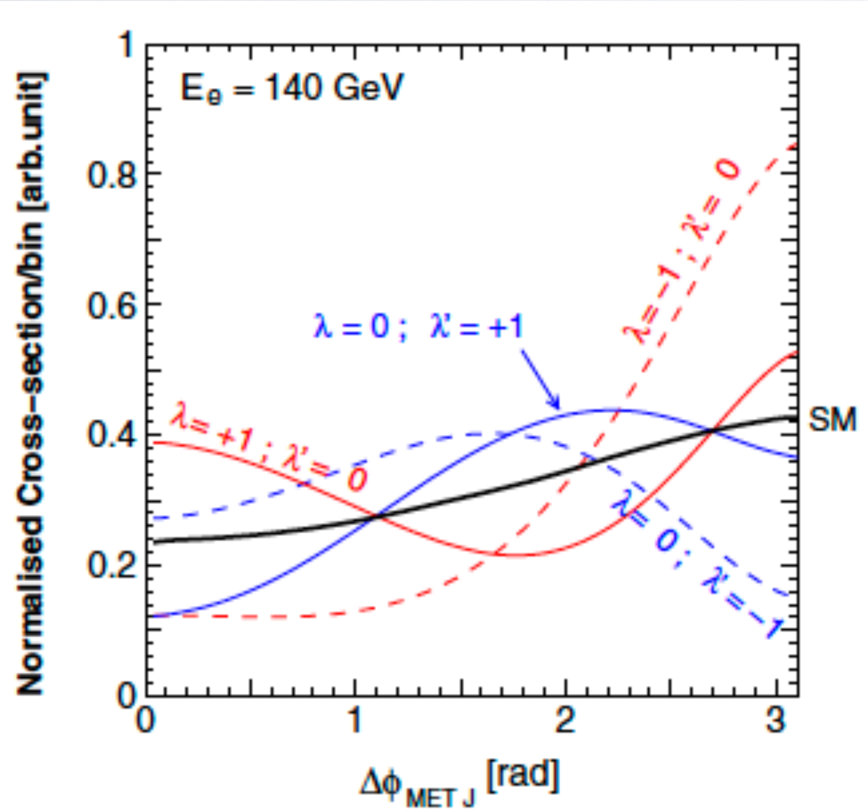

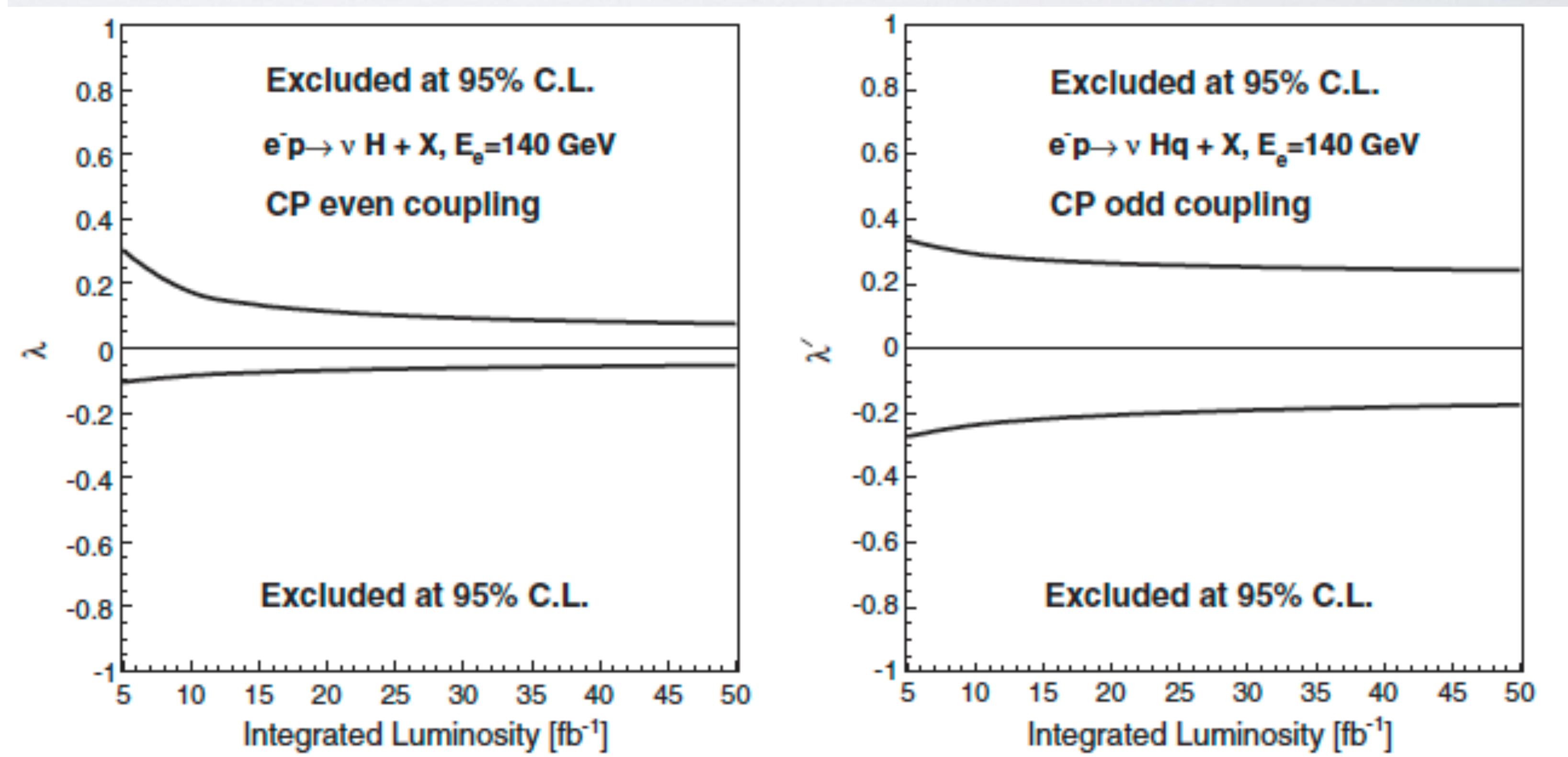

LHeC is the only machine where one can measure the HWW coupling directly without making any prior assumptions about new BSM physics.

III.

Physics Letters B 764 (2017) 247–253

Probing anomalous couplings using di-Higgs production in electron–proton collisions

Mukesh Kumar[a,*], Xifeng Ruan[b], Rashidul Islam[c], Alan S. Cornell[a], Max Klein[d], Uta Klein[d], Bruce Mellado[b]

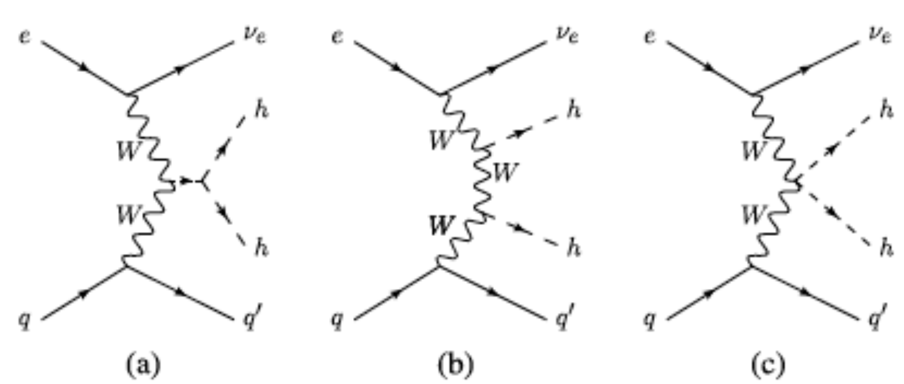

Fig. 1. Leading order diagrams contributing to the process $pe^- \to hhj\nu_e$ with $q \equiv u, c, \bar d, \bar s$ and $q' \equiv d, s, \bar u, \bar c$ respectively.

The complete Lagrangian we work with is as follows:

$$\mathcal{L} = \mathcal{L}_{SM} + \mathcal{L}^{(3)}_{hhh} + \mathcal{L}^{(3)}_{hWW} + \mathcal{L}^{(4)}_{hhWW}. \qquad (5)$$

The most general effective vertices take the form:

$$\Gamma_{hhh} = -6\lambda v\left[g^{(1)}_{hhh} + \frac{g^{(2)}_{hhh}}{3m_h^2}(p_1\cdot p_2 + p_2\cdot p_3 + p_3\cdot p_1)\right], \qquad (6)$$

$$\begin{aligned}\Gamma_{hW^-W^+} = g m_W\Bigg[&\left\{1+\frac{g^{(1)}_{hWW}}{m_W^2}p_2\cdot p_3 + \frac{g^{(2)}_{hWW}}{m_W^2}(p_2^2+p_3^2)\right\}\eta^{\mu_2\mu_3}\\ &- \frac{g^{(1)}_{hWW}}{m_W^2}p_2^{\mu_3}p_3^{\mu_2} - \frac{g^{(2)}_{hWW}}{m_W^2}(p_2^{\mu_2}p_2^{\mu_3} + p_3^{\mu_2}p_3^{\mu_3})\\ &- i\frac{\tilde g_{hWW}}{m_W^2}\epsilon_{\mu_2\mu_3\mu\nu}p_2^{\mu}p_3^{\nu}\Bigg], \qquad (7)\end{aligned}$$

$$\begin{aligned}\Gamma_{hhW^-W^+} = g^2\Bigg[&\left\{\frac{1}{2}+\frac{g^{(1)}_{hhWW}}{m_W^2}p_3\cdot p_4 + \frac{g^{(2)}_{hhWW}}{m_W^2}(p_3^2+p_4^2)\right\}\eta^{\mu_3\mu_4}\\ &- \frac{g^{(1)}_{hhWW}}{m_W^2}p_3^{\mu_4}p_4^{\mu_3} - \frac{g^{(2)}_{hhWW}}{m_W^2}(p_3^{\mu_3}p_3^{\mu_4} + p_4^{\mu_3}p_4^{\mu_4})\\ &- i\frac{\tilde g_{hhWW}}{m_W^2}\epsilon_{\mu_3\mu_4\mu\nu}p_3^{\mu}p_4^{\nu}\Bigg]. \qquad (8)\end{aligned}$$

$$V(\Phi) = \mu^2\Phi^\dagger\Phi + \lambda(\Phi^\dagger\Phi)^2 \to \frac{1}{2}m_h^2h^2 + \lambda v h^3 + \frac{\lambda}{4}h^4, \qquad (1)$$

$$\mathcal{L}^{(3)}_{hhh} = \frac{m_h^2}{2v}(1-g^{(1)}_{hhh})h^3 + \frac{1}{2v}g^{(2)}_{hhh}h\partial_\mu h\partial^\mu h, \qquad (2)$$

$$\begin{aligned}\mathcal{L}^{(3)}_{hWW} = -g\Bigg[&\frac{g^{(1)}_{hWW}}{2m_W}W^{\mu\nu}W^\dagger_{\mu\nu}h + \frac{g^{(2)}_{hWW}}{m_W}(W^\nu\partial^\mu W^\dagger_{\mu\nu}h + \text{h.c})\\ &+ \frac{\tilde g_{hWW}}{2m_W}W^{\mu\nu}\widetilde W^\dagger_{\mu\nu}h\Bigg], \qquad (3)\end{aligned}$$

$$\begin{aligned}\mathcal{L}^{(4)}_{hhWW} = -g^2\Bigg[&\frac{g^{(1)}_{hhWW}}{4m_W^2}W^{\mu\nu}W^\dagger_{\mu\nu}h^2\\ &+ \frac{g^{(2)}_{hhWW}}{2m_W^2}(W^\nu\partial^\mu W^\dagger_{\mu\nu}h^2 + \text{h.c})\\ &+ \frac{\tilde g_{hhWW}}{4m_W^2}W^{\mu\nu}\widetilde W^\dagger_{\mu\nu}h^2\Bigg]. \qquad (4)\end{aligned}$$

Table 1
Cross sections of signal and backgrounds in charged current (cc), neutral current (nc) and photo-production (photo) modes for $E_e = 60$ GeV and $E_p = 50$ TeV, where j is light quarks and gluons. For this estimation we use basic cuts $|\eta| \le 10$ for light-jets, leptons and b-tagged jets, $p_T \ge 10$ GeV, $\Delta R_{min} = 0.4$ for all particles. And electron polarisation is taken to be −0.8.

Process	cc (fb)	nc (fb)	photo (fb)
Signal:	2.40×10^{-1}	3.95×10^{-2}	3.30×10^{-6}
$bbbbj$:	8.20×10^{-1}	$3.60 \times 10^{+3}$	$2.85 \times 10^{+3}$
$b\bar b jjj$:	$6.50 \times 10^{+3}$	$2.50 \times 10^{+4}$	$1.94 \times 10^{+6}$
ZZj ($Z \to b\bar b$):	7.40×10^{-1}	1.65×10^{-2}	1.73×10^{-2}
$t\bar t j$ (hadronic):	3.30×10^{-1}	$1.40 \times 10^{+2}$	$3.27 \times 10^{+2}$
$t\bar t j$ (semi-leptonic):	1.22×10^{-1}	$4.90 \times 10^{+1}$	$1.05 \times 10^{+2}$
$hb\bar b j$ ($h \to b\bar b$):	5.20×10^{-1}	1.40×10^{0}	2.20×10^{-2}
hZj ($Z, h \to b\bar b$):	6.80×10^{-1}	9.83×10^{-3}	6.70×10^{-3}

Optimisation of Events

Table 2
A summary table of event selections to optimise the signal with respect to the backgrounds in terms of the weights at 10 ab^{-1}. In the first column the selection criteria are given as described in the text. The second column contains the weights of the signal process $pe^- \rightarrow hhj\nu_e$, where both the Higgs bosons decay to $b\bar{b}$ pair. In the next columns the sum of weights of all individual prominent backgrounds in charged current, neutral current and photo-production are given with each selection, whereas in the penultimate column all backgrounds' weights are added. The significance is calculated at each stage of the optimised selection criteria using the formula $\mathcal{S} = \sqrt{2[(S+B)\log(1+S/B) - S]}$, where S and B are the expected signal and background yields at a luminosity of 10 ab^{-1} respectively. This optimisation has been performed for $E_e = 60$ GeV and $E_p = 50$ TeV.

Cuts/Samples	Signal	$4b+$ jets	$2b+$ jets	Top	ZZ	$b\bar{b}H$	ZH	Total Bkg	Significance
Initial	2.00×10^3	3.21×10^7	2.32×10^9	7.42×10^6	7.70×10^3	1.94×10^4	6.97×10^3	2.36×10^9	0.04
At least $4b + 1j$	3.11×10^2	7.08×10^4	2.56×10^4	9.87×10^3	7.00×10^2	6.32×10^2	7.23×10^2	1.08×10^5	0.94
Lepton rejection $p_T^\ell > 10$ GeV	3.11×10^2	5.95×10^4	9.94×10^3	6.44×10^3	6.92×10^2	2.26×10^2	7.16×10^2	7.75×10^4	1.12
Forward jet $\eta_J > 4.0$	233	13007.30	2151.15	307.67	381.04	46.82	503.22	16397.19	1.82
$\not{E}_T > 40$ GeV	155	963.20	129.38	85.81	342.18	19.11	388.25	1927.93	3.48
$\Delta\phi_{\not{E}_T j} > 0.4$	133	439.79	61.80	63.99	287.10	14.53	337.14	1204.35	3.76
$m_{bb}^1 \in [95, 125]$, $m_{bb}^2 \in [90, 125]$	54.5	28.69	5.89	6.68	5.14	1.42	17.41	65.23	6.04
$m_{4b} > 290$ GeV	49.2	10.98	1.74	2.90	1.39	1.21	11.01	29.23	7.51

We base our simulation on the following kinematic selections in order to optimise the significance of the SM signal over all the backgrounds: (1) At least four b-tagged jets and one additional light jet are selected in an event with transverse momenta, p_T, greater than 20 GeV. (2) For *non*-b-tagged jets, the absolute value of the rapidity, $|\eta|$, is taken to be less than 7, whereas for b-tagged jets it is less than 5. (3) The four b-tagged jets must be well separated and the distance between any two jets, defined as $\Delta R = \sqrt{(\Delta\phi)^2 + (\Delta\eta)^2}$, ϕ being the azimuthal angle, is taken to be greater than 0.7. (4) Charged leptons with $p_T > 10$ GeV are rejected. (5) For the largest p_T forward jet J (the *non*-b-tagged jet after selecting at least four b-jets) $\eta_J > 4.0$ is required. (6) The missing transverse energy, $\not{E}_T$, is taken to be greater than 40 GeV.

(7) The azimuthal angle between $\not{E}_T$ and the b-tagged jets are: $\Delta\Phi_{\not{E}_T,\ leading\ jet} > 0.4$ and $\Delta\Phi_{\not{E}_T,\ sub-leading\ jet} > 0.4$. (8) The four b-tagged jets are grouped into two pairs such that the distances of each pair to the true Higgs mass are minimised. The leading mass contains the leading p_T-ordered b-jet. The first pair is required to be within 95–125 GeV and the second pair within 90–125 GeV.[5] (9) The invariant mass of all four b-tagged jets has to be greater than 290 GeV.

In the selections (described above) the b-tagging efficiency is assumed to be 70%, with fake rates from c-initiated jets and light jets to the b-jets of 10% and 1% respectively. Corresponding weights[6] at a particular luminosity of 10 ab^{-1} for a signal, and all backgrounds with significance has been tabulated in Table 2. Significance at all stages of the cuts are calculated using the Poisson formula $\mathcal{S} = \sqrt{2[(S+B)\log(1+S/B) - S]}$, where S and B are the expected signal and background yields at a particular luminosity respectively.

Azimuthal Angle correlations and Asymmetries

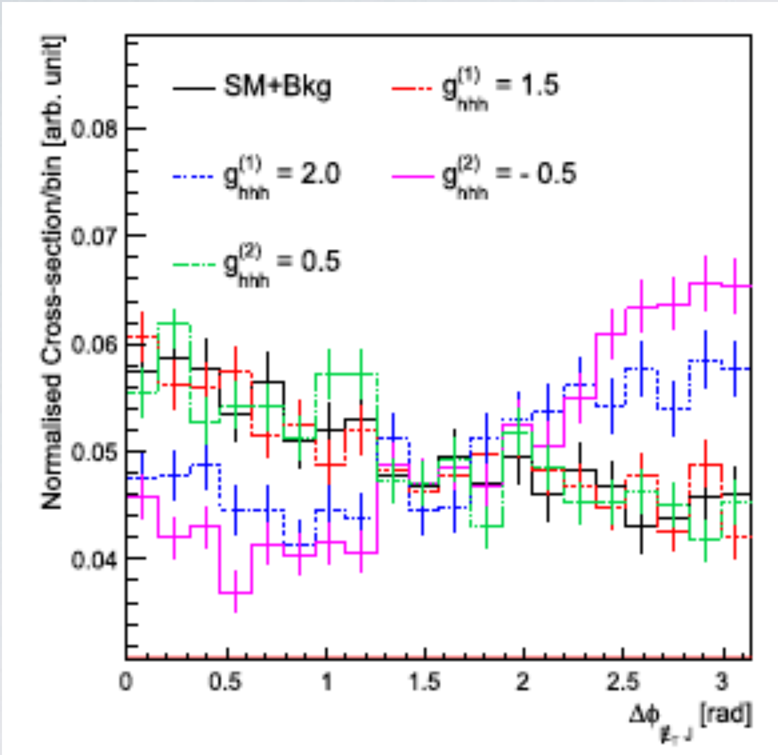

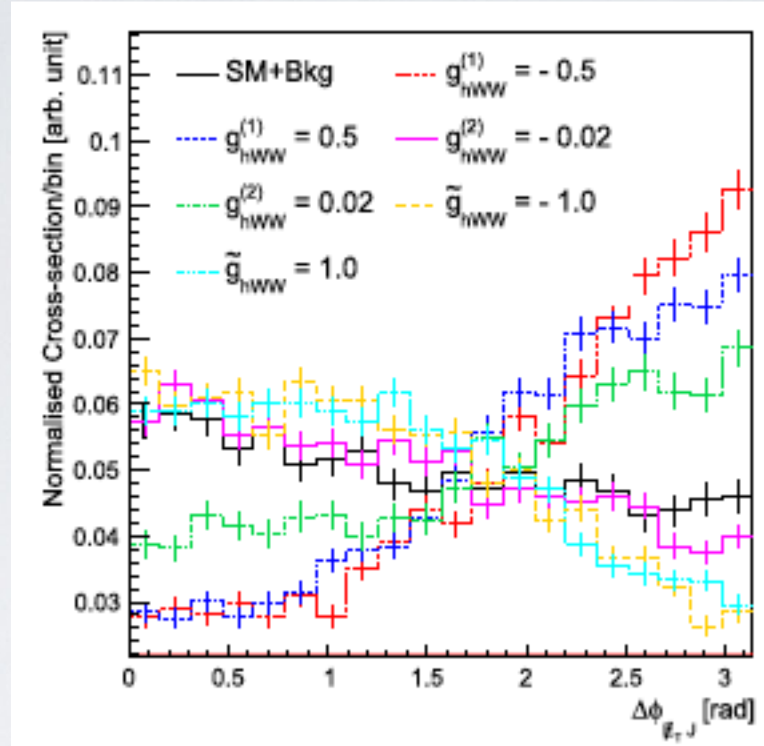

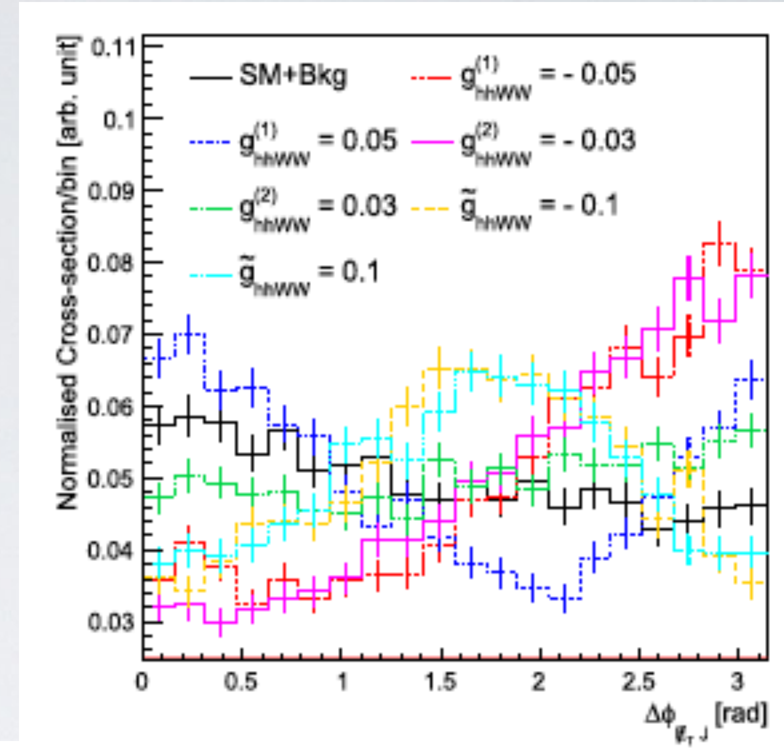

Choice of couplings are ad-hoc though these values are derived at 0.4 /ab based on cross sections.
[M. Kumar, J. Phys. Conf. Ser. 645, no. 1, 012005 (2015), arXiv: 1506.03999]

$$\mathcal{A}_{\Delta\phi_{\not{E}_T J}} = \frac{|A_{\Delta\phi>\pi/2}| - |A_{\Delta\phi<\pi/2}|}{|A_{\Delta\phi>\pi/2}| + |A_{\Delta\phi<\pi/2}|}$$

Table 3
Estimation of the asymmetry, defined in Eq. (9), and statistical error associated with the kinematic distributions in Fig. 2 at an integrated luminosity of 10 ab^{-1}. The cross section (σ) for the corresponding coupling choice is given in the last column with same parameters as in Table 1.

Samples		$\mathcal{A}_{\Delta\phi_{\not{E}_T J}}$	σ (fb)
SM+Bkg		0.277 ± 0.088	
$g^{(1)}_{hhh}$	$= 1.5$	0.279 ± 0.052	0.18
	$= 2.0$	0.350 ± 0.053	0.21
$g^{(2)}_{hhh}$	$= -0.5$	0.381 ± 0.050	0.19
	$= 0.5$	0.274 ± 0.024	0.74
$g^{(1)}_{hWW}$	$= -0.5$	0.506 ± 0.022	0.88
	$= 0.5$	0.493 ± 0.020	0.94
$g^{(2)}_{hWW}$	$= -0.02$	0.257 ± 0.025	0.67
	$= 0.02$	0.399 ± 0.040	0.33
$\tilde{g}_{hWW}$	$= -1.0$	0.219 ± 0.016	1.53
	$= 1.0$	0.228 ± 0.016	1.53
$g^{(1)}_{hhWW}$	$= -0.05$	0.450 ± 0.033	0.52
	$= 0.05$	0.254 ± 0.029	0.68
$g^{(2)}_{hhWW}$	$= -0.03$	0.462 ± 0.022	1.22
	$= 0.03$	0.333 ± 0.018	1.46
$\tilde{g}_{hhWW}$	$= -0.1$	0.351 ± 0.020	1.60
	$= 0.1$	0.345 ± 0.020	1.61

Exclusion Limits of couplings at FCC-he: Ee = 60 GeV, Ep = 50 TeV

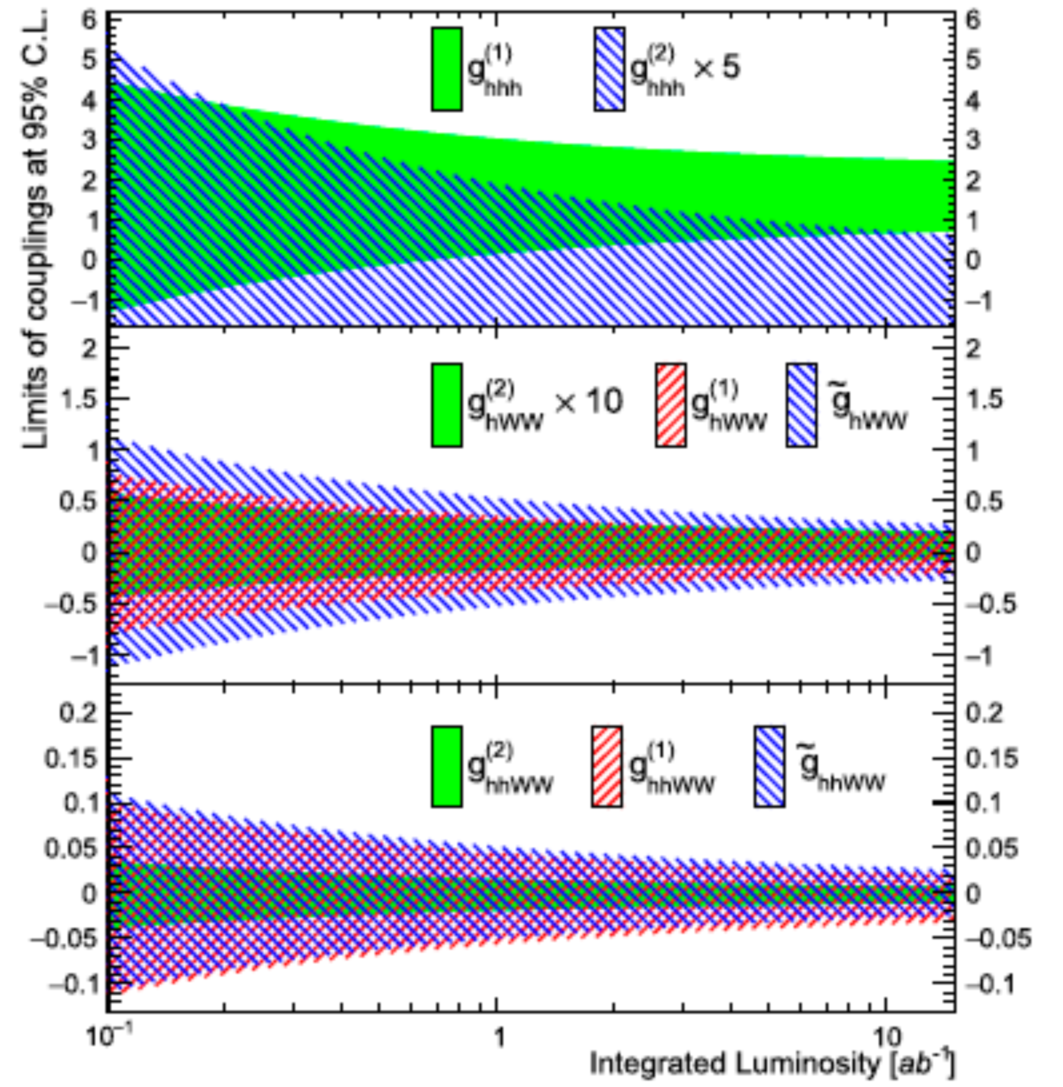

Fig. 3. The exclusion limits on the anomalous *hhh* (top panel), *hWW* (middle panel) and *hhWW* (lower panel) couplings at 95% C.L. as a function of integrated luminosity (shaded areas). Note that the allowed values of $g^{(2)}_{hhh}$ and $g^{(2)}_{hWW}$ are multiplied by 5 and 10 respectively to highlight their exclusion region, since the values are of the order 10^{-1}.

Degradation of anomalous couplings w.r.t scale of higher dimensional operators:

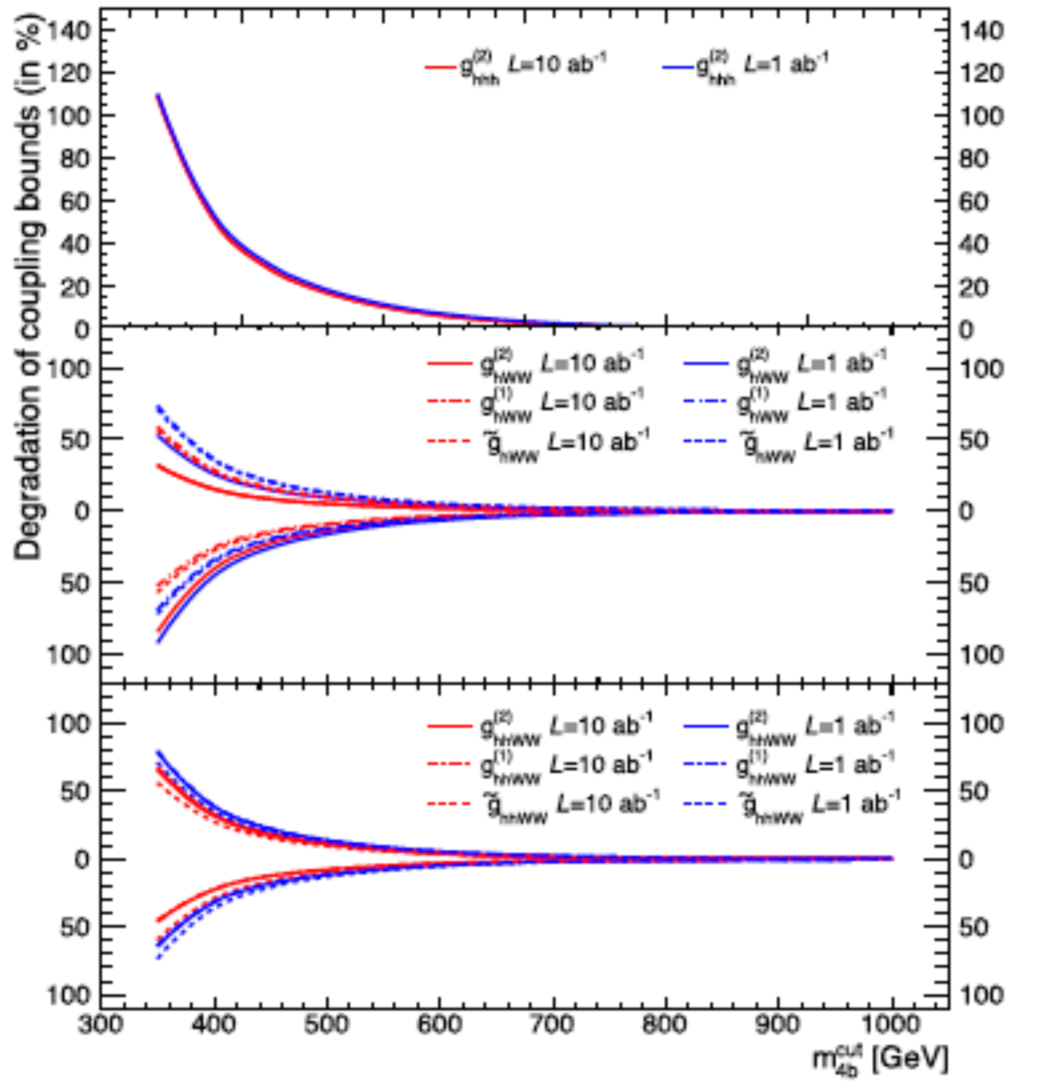

Fig. 4. Percentage of deterioration of exclusion limits of anomalous tensorial couplings (shown in Fig. 3) with respect to the upper di-Higgs invariant mass cut $m'_{4b} \equiv m^{cut}_{4b}$ [in GeV] for fixed luminosity of 1 ab^{-1} (*blue*) and 10 ab^{-1} (*red*). The numbers in the vertical axis above (below) 0 is the degradation in the upper (lower) limits. (For interpretation of the references to colour in this figure legend, the reader is referred to the web version of this article.)

$$g^{(1)}_{hhh} = 1.00^{+0.24(0.14)}_{-0.17(0.12)} \text{ at } \sqrt{s} = 3.5(5.0) \text{ TeV for an ultimate } 10 \text{ ab}^{-1}$$

IV.

Measuring CP nature of top-Higgs couplings at the future Large Hadron electron collider

Baradhwaj Coleppa[a], Mukesh Kumar[b], Satendra Kumar[a], Bruce Mellado[c]

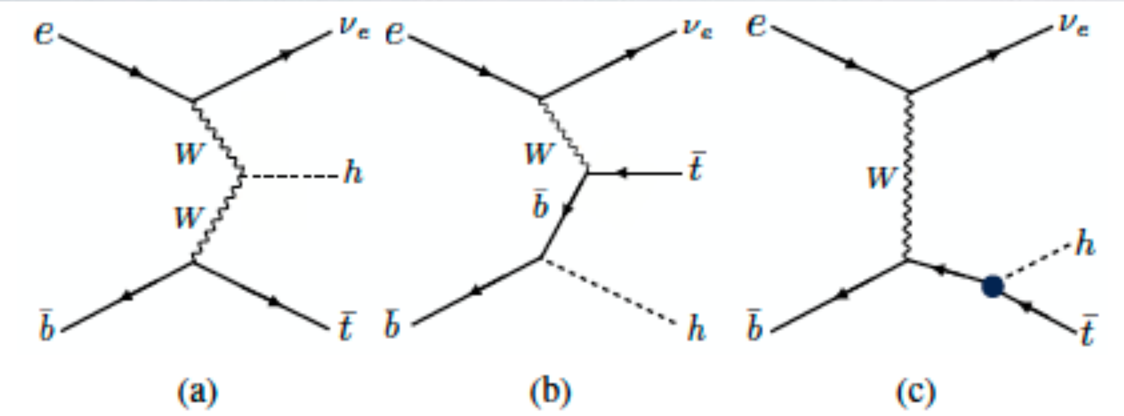

Figure 1: Leading order Feynman diagrams contributing to the process $p e^- \to \bar{t} h \nu_e$ at the LHeC. The black dot in the Feynman diagram (c) denotes the top-Higgs coupling which is the subject of this study.

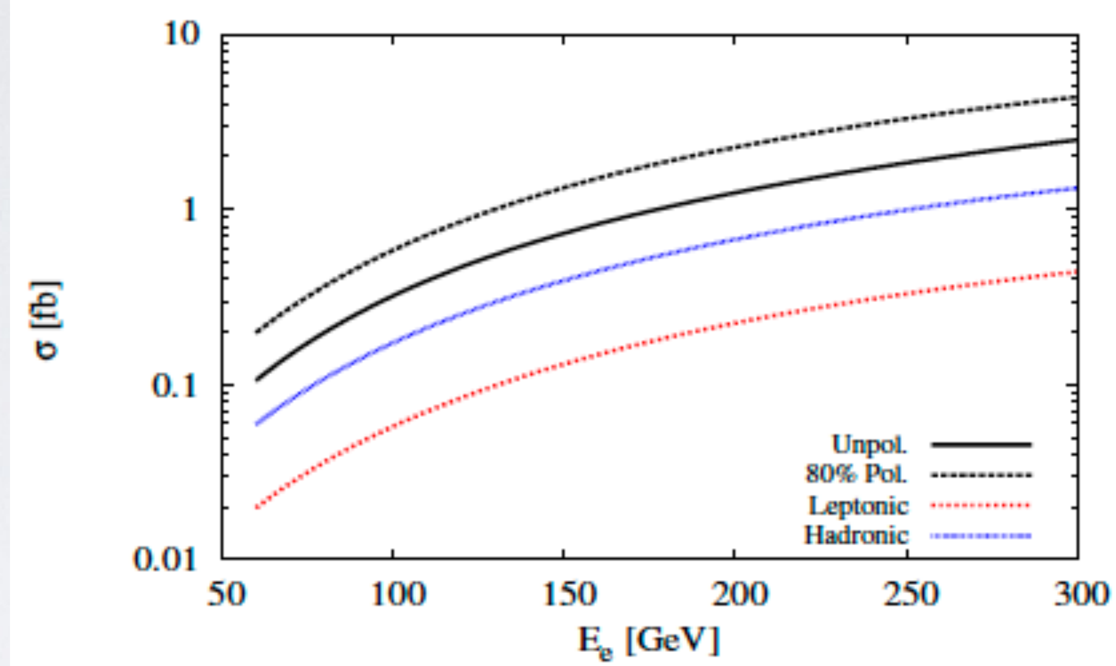

All analyses at Parton level

Process	CC (fb)	NC (fb)	PHOTO (fb)
Signal:	1.98×10^{-2}	--	--
$Wjjj + X$, \h	$2.05 \times 10^{+2}$	$3.18 \times 10^{+1}$	$3.40 \times 10^{+3}$
$Wjjj + X$, \t	$4.18 \times 10^{+1}$	$3.16 \times 10^{+1}$	$3.41 \times 10^{+3}$
$Wjjj + X$, \th	$4.16 \times 10^{+1}$	$3.18 \times 10^{+1}$	$3.41 \times 10^{+3}$

Table 1: Cross sections of signal and backgrounds in charged current (CC), neutral current (NC) and photo-production (PHOTO) modes for E_e = 60 GeV and E_p = 7 TeV as explained in the text. Here X could be either of missing energy or electron and j is all possible combinations of light-, c- and b-quarks and gluons. For this estimation we use basic cuts as mentioned in text and electron polarisation is taken to be – 0.8.

Observables:

$$\mathcal{L} = -i\frac{m_t}{v}\bar{t}\,[\kappa \cos\zeta_t + i\gamma_5 \sin\zeta_t]\,t\,h$$

1. Cross section

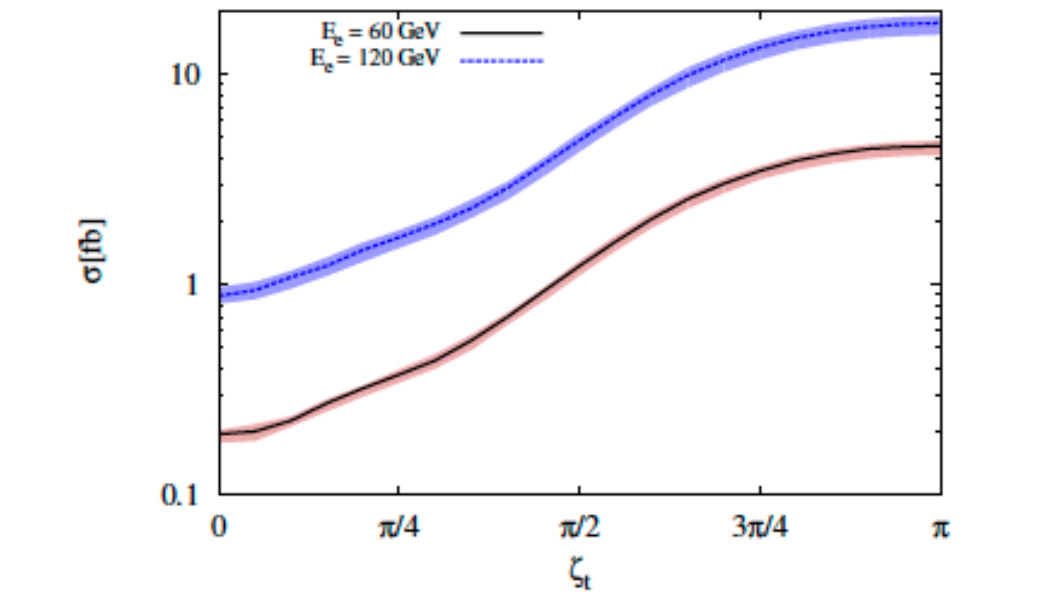

Figure 3: Total cross section as a function of ζ_t with scale uncertainties. The *black* solid and *blue* dotted lines correspond to $E_e = 60$ and 120 GeV respectively for fixed $E_p = 7$ TeV and $\mu_F = \mu_R = (m_t + m_h)/4$.

2. Rapidity difference

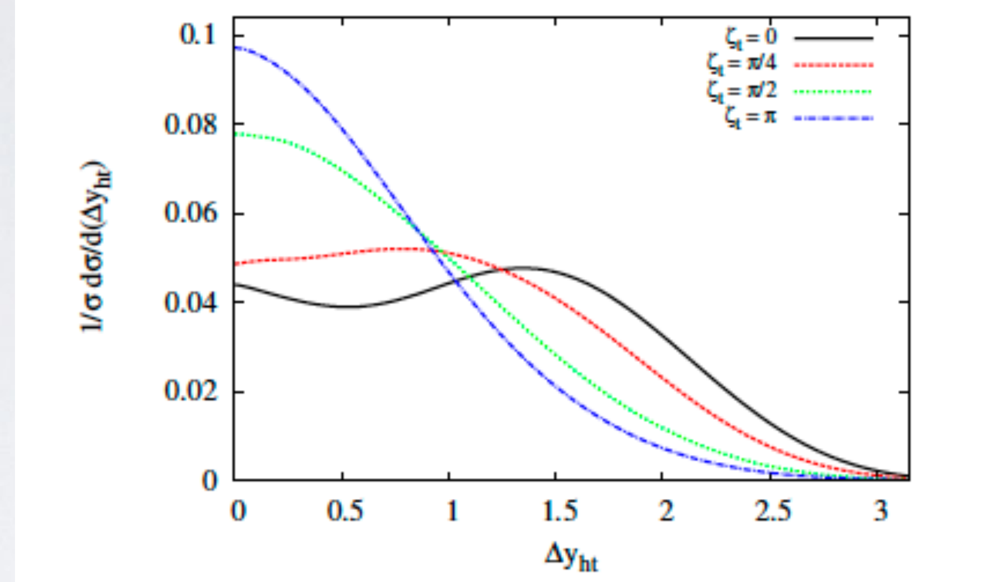

Figure 4: The normalised difference between rapidities of top quark and the Higgs boson at some typical values of ζ_t for $E_e = 60$ GeV and $E_p = 7$ TeV. The *black* solid line corresponds to the SM case, while dotted lines correspond to different values of ζ_t.

3. Top-Quark Polarisation

$$P_t = \frac{N_+ - N_-}{N_+ + N_-} \equiv \frac{\sigma_+ - \sigma_-}{\sigma_+ + \sigma_-}$$

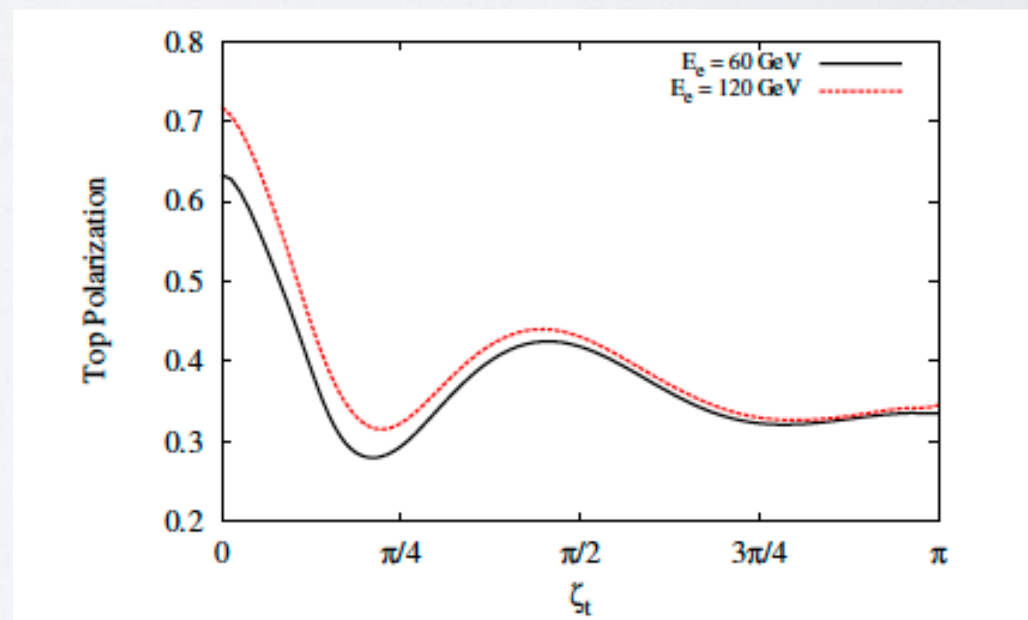

Figure 5: The degree of longitudinal polarisation (P_t) of the top quark against ζ_t. The *black* solid and *red* dotted lines correspond to the $E_e =$ 60 and 120 GeV, while E_p is fixed at 7 TeV.

$$\frac{1}{\Gamma_f}\frac{d\Gamma_f}{d\cos\theta_f} = \frac{1}{2}(1 + \alpha_f P_t \cos\theta_f),$$

4. Asymmetries

$$A_{\theta_{ij}} = \frac{N_+^A(\cos\theta_{ij} > 0) - N_-^A(\cos\theta_{ij} < 0)}{N_+^A(\cos\theta_{ij} > 0) + N_-^A(\cos\theta_{ij} < 0)},$$

$$A_{\Delta\phi_{ij}} = \frac{N_+^A(\Delta\phi_{ij} > \pi/2) - N_-^A(\Delta\phi_{ij} < \pi/2)}{N_+^A(\Delta\phi_{ij} > \pi/2) + N_-^A(\Delta\phi_{ij} < \pi/2)}$$

$$\delta_\alpha = \sqrt{\frac{1 - A_\alpha^2(\zeta_t)}{\sigma_{\zeta_t} \cdot L}}, \qquad (\alpha = \theta_{ij}, \Delta\phi_{ij})$$

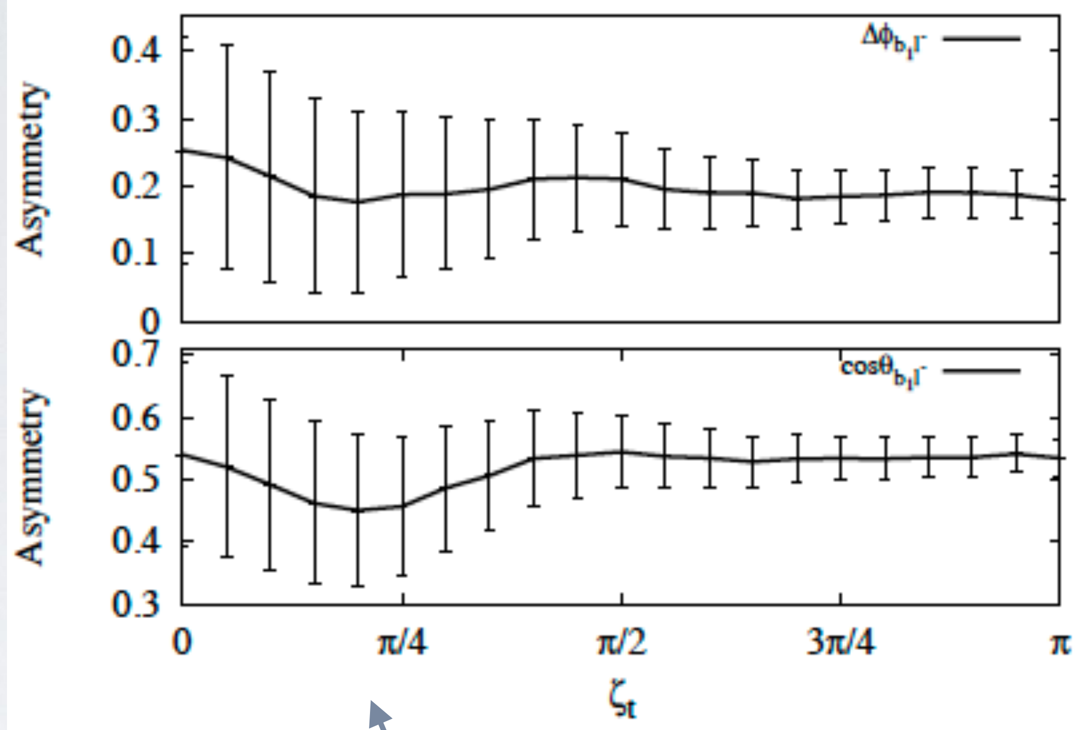

Figure 6: Variation of angular asymmetries between the leading b-tagged jet and the charged lepton in the differential azimuthal and polar angle ($\Delta\phi_{b_1 l^-}$ and $\cos\theta_{b_1 l^-}$) distributions with respect to ζ_t for $E_e = 60$ GeV and $E_p = 7$ TeV. The error bars correspond to the uncertainties in asymmetry measurement at $L = 1\ \text{ab}^{-1}$.

Follow the top-quark polarisation pattern

Optimising Events:

(1) $p_T \geq 20(10)$ GeV b-tagged jets and light jets (leptons)

(2) $-2 \leq \eta \leq 5 (2 \leq \eta \leq 5)$ b-tagged jets (light jets and leptons)

(3) $\Delta R > 0.4$

(4) $E_T > 10$ (GeV)

(5) $115 < m_{bb} < 130$ (GeV), $160 < \mathrm{m_t} < 177$ (GeV)

$b-$tagging efficiency is assumed to be 70%, fake rates from
$c-$initiated jets and light jets to the b-jets to be 10% and 1%.

Exclusion Limits:

Based on Asymmetry

$$\delta A_{\cos\theta_{b_2 l^-}} = \sqrt{\frac{1-(A^{SM}_{\cos\theta_{b_2 l^-}})^2}{\sigma_{SM}\cdot L}},$$

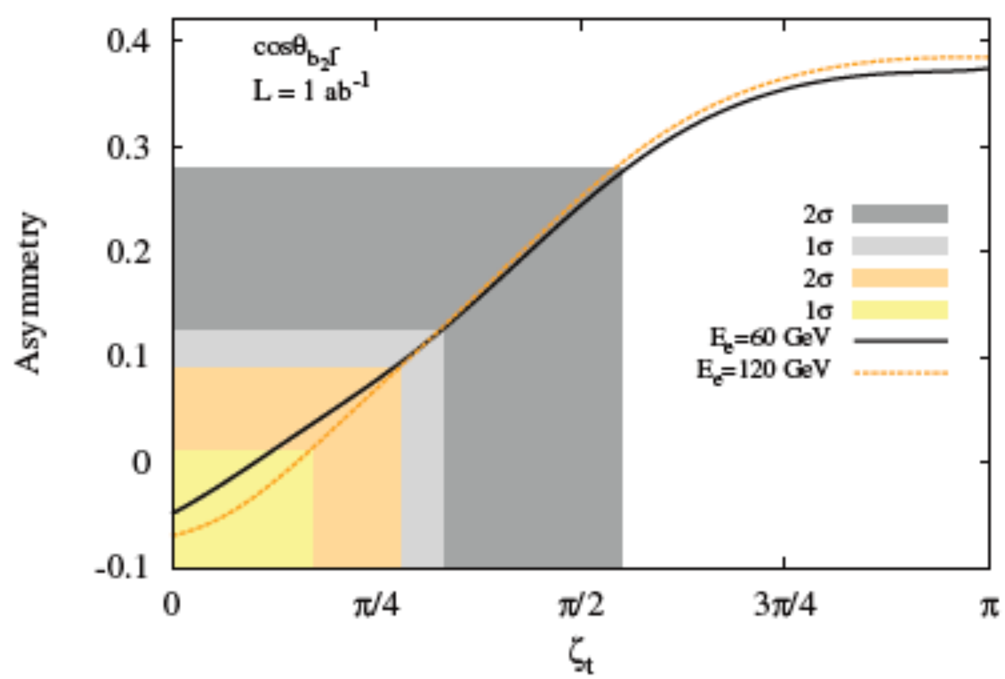

Figure 7: Variation of the angular asymmetry between the subleading b-tagged jets and charged leptons in the differential polar angle ($\cos\theta_{b_2 l^-}$) distribution with respect to ζ_t for E_e = 60 GeV (*black* solid line) and E_e = 120 GeV (*orange* dashed line) with E_p = 7 TeV. The shaded regions *grey* (*orange*) and *light grey* (*yellow*) corresponds to 2σ and 1σ of statistical uncertainty in the measurement of the asymmetry in the SM for $E_e = 60\,(120)$ GeV at $L = 1\ \text{ab}^{-1}$ respectively.

Based on Fiducial Cross Section

$$\mathcal{S} = \sqrt{2[(S+B)\log(1+S/B)-S]}$$

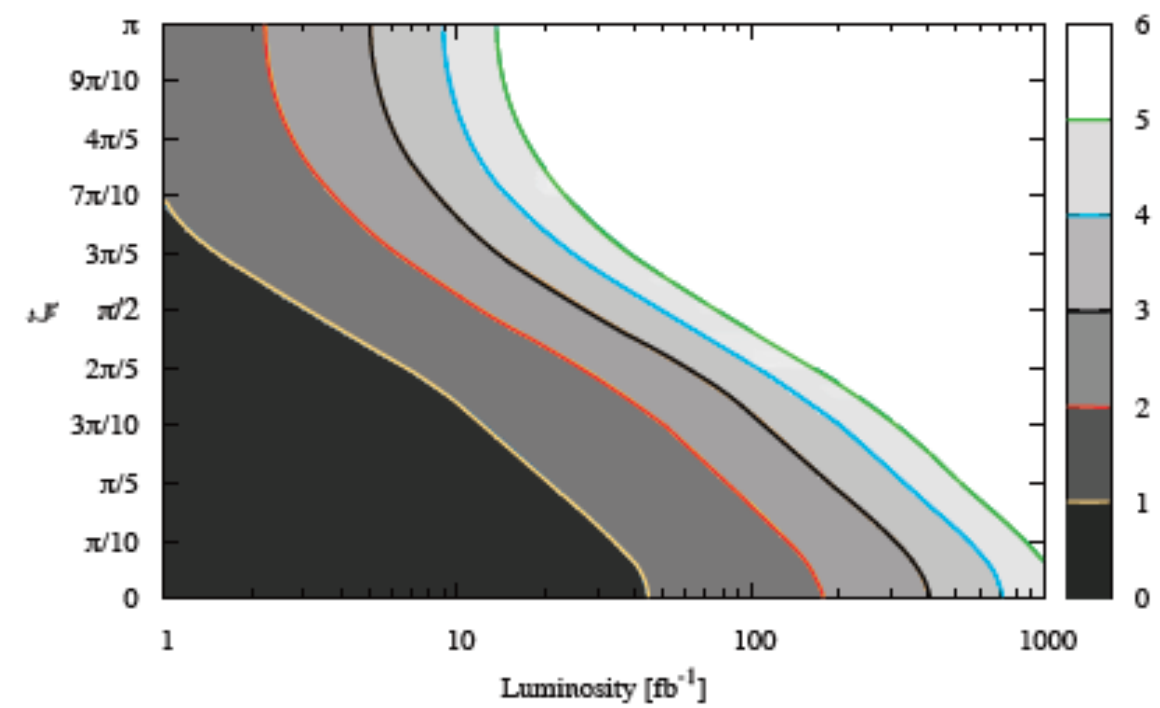

Figure 8: The exclusion contour with respect to integrated luminosities at various ζ_t by considering significance based on fiducial cross section (defined in text) for E_e = 60 GeV and E_p = 7 TeV. The regions beyond each contours are excluded for the particular luminosity, *black* and *red* solid lines correspond to 3σ and 2σ regions.

accuracy of SM tth coupling κ at the LHeC energies. To measure the accuracy of κ by using signal and background yields we use the formula $\mathcal{K} = \sqrt{(S+B)}/(2S)$ at a particular luminosity. And for $E_e = 60\,(120)$ GeV, the measured accuracy at the design luminosity $L = 1\ \text{ab}^{-1}$ is given to be $\kappa = 1.00 \pm 0.17\,(0.08)$ of its expected SM value, where a 10% systematic uncertainty is been taken in background yields only.

V. Higgs Invisible decay at the LHeC and FCC-he

[S. Kawaguchi / M. Kuze (Tokyo Tech)]

Motivated by parton-level study by
Y.L.Tang, C.Zhang and S.Zhu, Phys. Rev. D 94, 011702 (2016)

CC production

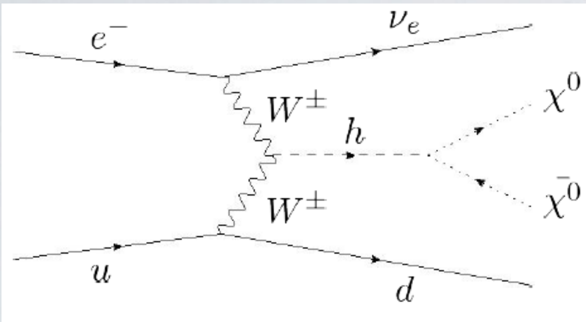

NC production

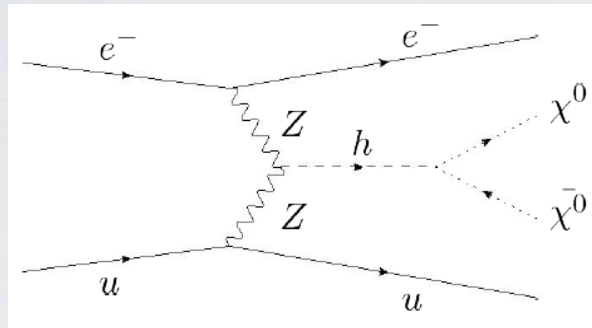

- Focus currently on NC: both jet and electron information are available for analysis.
- Emulate Higgs invisible decay by SM process NC: assumed a branching ratio of 100% $H \to ZZ \to 4\nu_l$
- Simulation and analyses based on LHeC and FCC-he configuration using **DELPHES**.

LHeC

FCC-he

Cut0 : $N_j \geq 1, N_e \geq 1; p_T > 20GeV, |\eta| < 5.0$ and $\Delta R > 0.4$ for leading jet and electron

LHeC

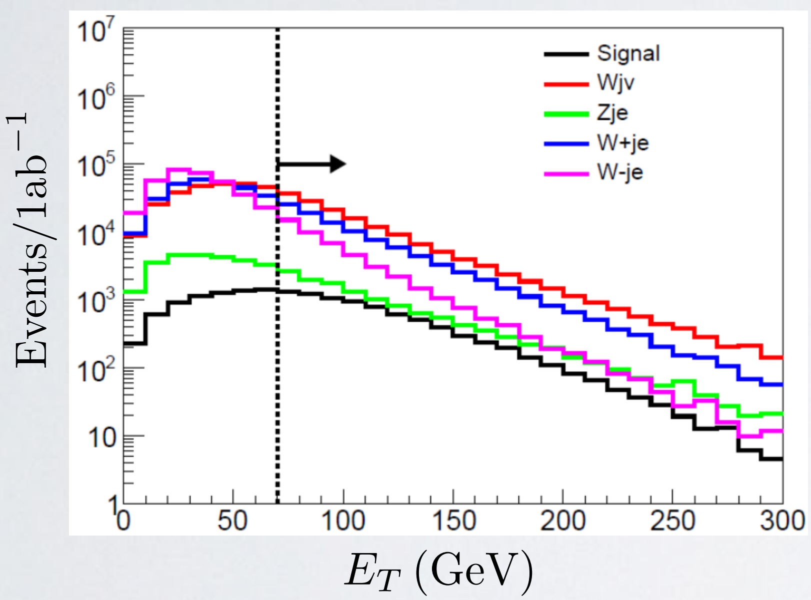

Cut1 : $|\phi_j - \phi_{E_T}| > 1.4\,\mathrm{rad}$
Cut2 : $E_T > 70\,\mathrm{GeV}$
Cut3 : $(\eta_j - \eta_e) > 2.5$
Cut4 : $|\phi_j - \phi_e| < 2\,\mathrm{rad}$
Cut5 : $-1.0 < \eta_e < 1.2$
Cut6 : $0.11 < y_e < 0.6$
Cut7 : require 1 electron, 1 jet, veto τ and μ

FCC-he

Cut1 : $|\phi_j - \phi_{E_T}| > 1.3\,\mathrm{rad}$
Cut2 : $E_T > 70\,\mathrm{GeV}$
Cut3 : $(\eta_j - \eta_e) > 3.5$
Cut4 : $|\phi_j - \phi_e| < 2.1\,\mathrm{rad}$
Cut5 : $-1.2 < \eta_e < 1.2$
Cut6 : $0.09 < y_e < 0.5$
Cut7 : require 1 electron, 1 jet, veto τ and μ

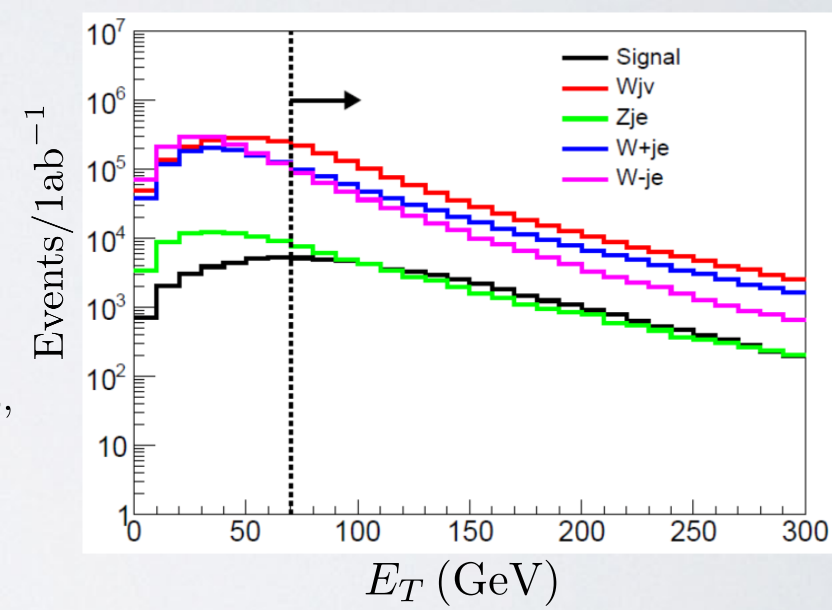

2σ sensitivity to branching ratio limits are (calculated using $S/\sqrt{S+B}$)

LHeC: $Br(h \to E_T) \sim 7.1\%$

FCC-he: $Br(h \to E_T) \sim 2.8\%$

***Statistical error only**

LHeC   FCC-he

Invariant mass distribution M_{ej} (GeV)   (Scaling the signal with 10% BR)

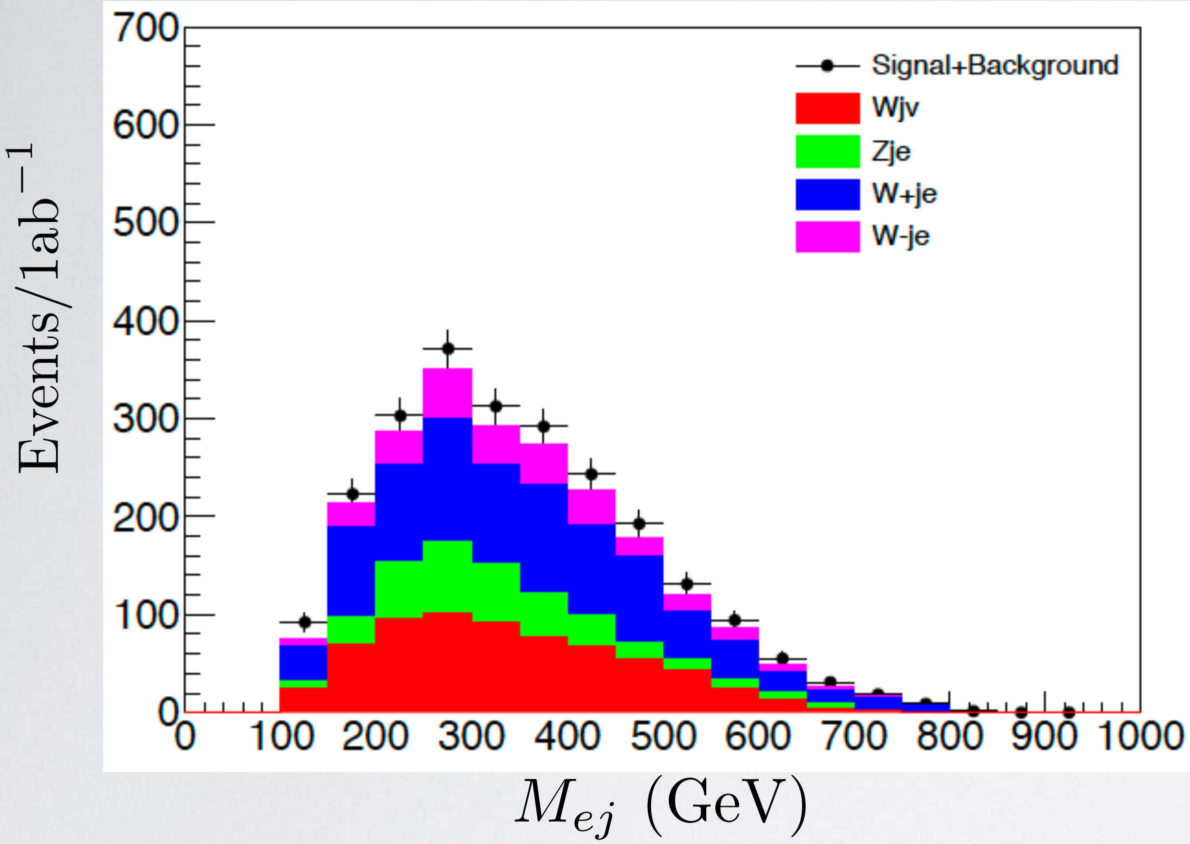

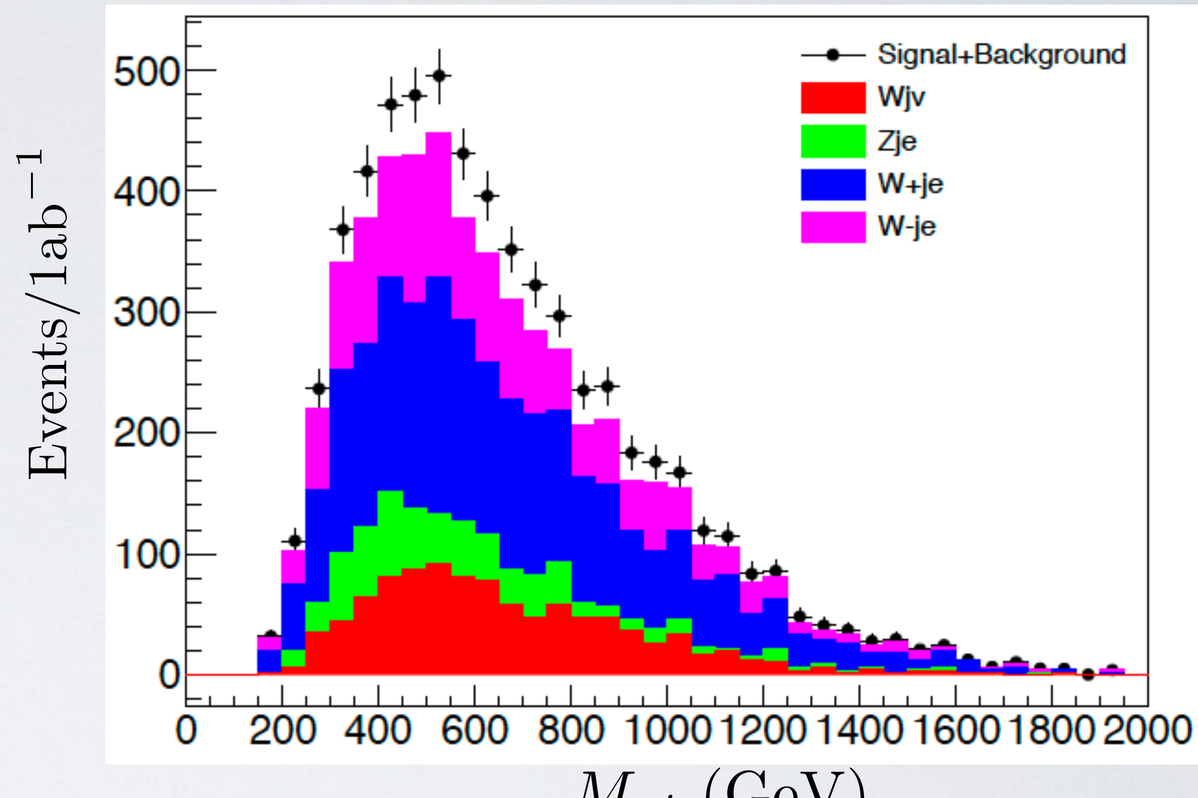

MVA (BDT) Analyses using 6 variables from Cut 1-6

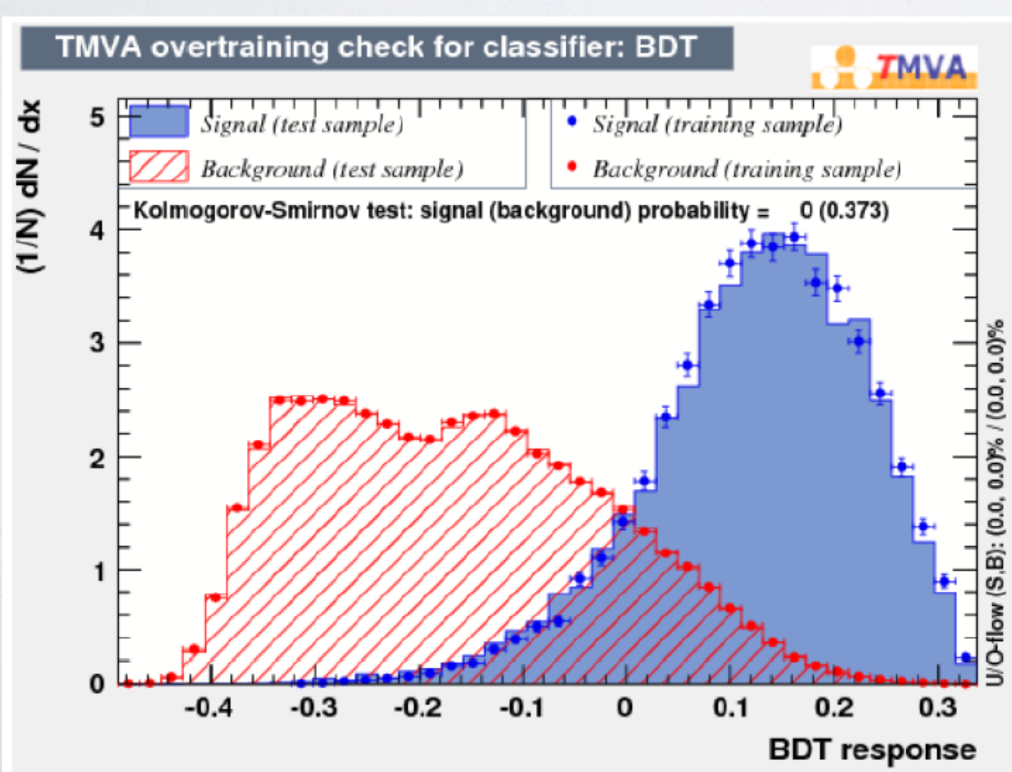

$Br(h \to E_T) \sim 6.1\%$

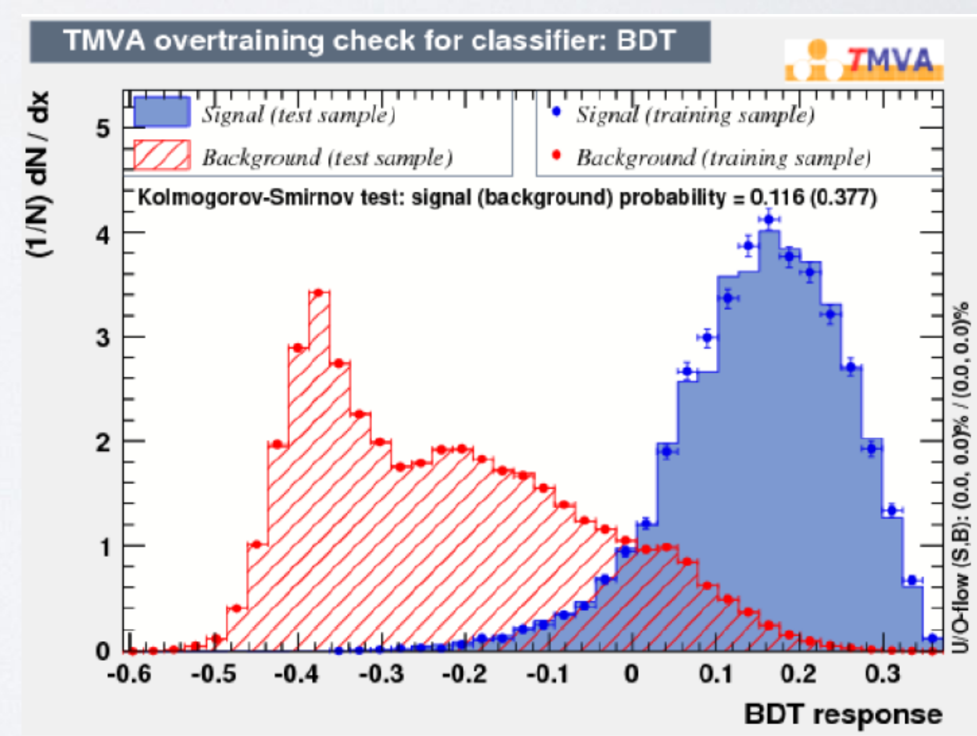

$Br(h \to E_T) \sim 2.4\%$

VI. Two-Higgs doublet Model at e-p collider

[Kumar et. al. Wits. Univ.]

Preliminary studies

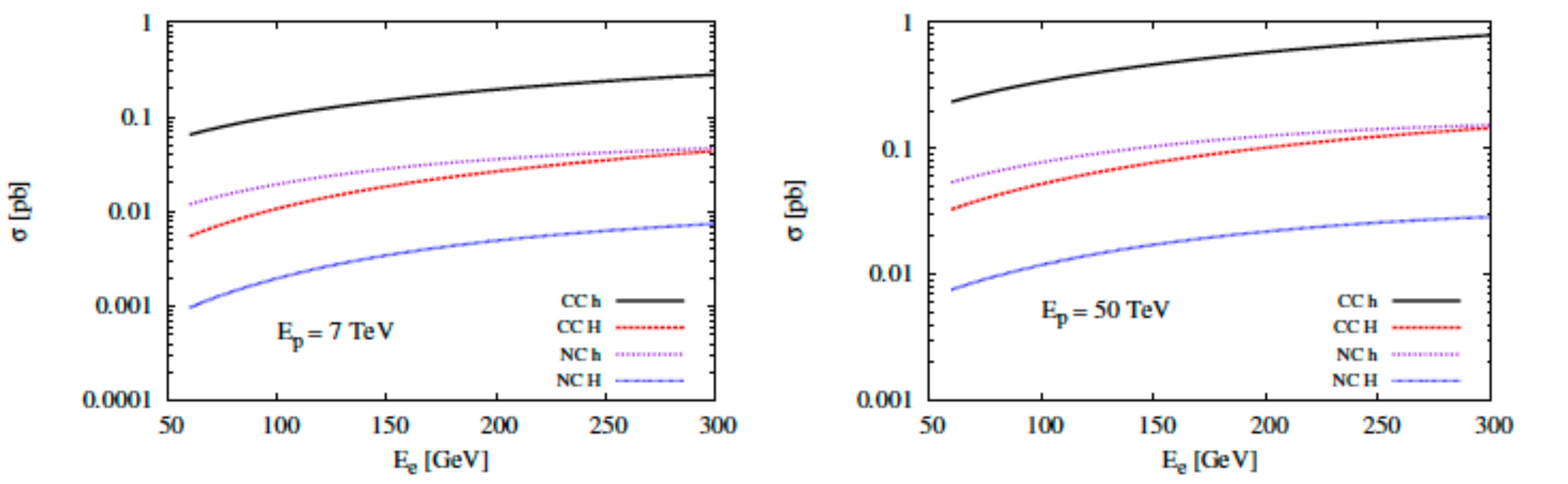

Figure 1. Production cross sections of h and H in charged and neutral current THDM Type-I with respect to electron beam energies E_e for fixed proton beam energy of $E_p = 7$ TeV (*left*) and $E_p = 50$ TeV (*right*). The default model parameters are as explained in the text with $\beta = 1.0$.

$m_h = 125, m_H = 270, m_A = 450,$
$m_{H^\pm} = 400$ GeV
$\beta = 1.0, \alpha = 3.13$
$\lambda_1 = 0.1, \lambda_2 = 0.27, \lambda_3 = 1.1,$
$\lambda_4 = -0.5, \lambda_5 = 0.5.$

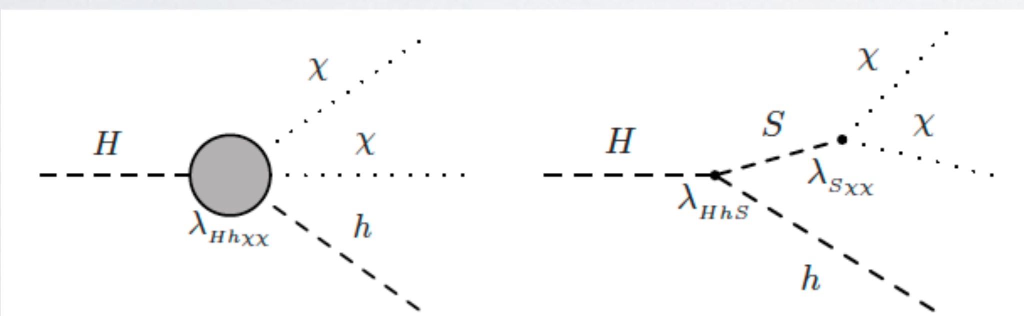

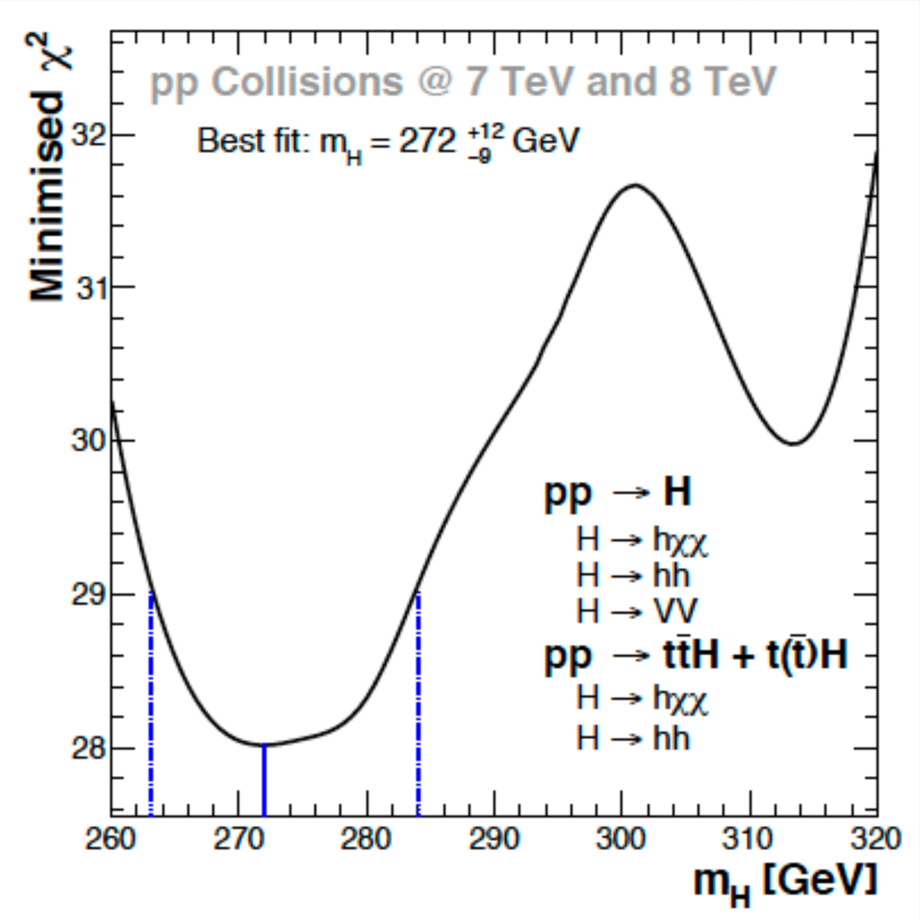

[ArXiv:1506.00612, 1603.01208, 1606.01674, 1608.03466]

Best Fit results: mH = 272+12-9 GeV

Investigating CP nature of $h\tau^+\tau^-$ coupling at the LHeC/FCC-he

[Kumar et. al. Wits. Univ.]

Preliminary studies

$$\mathcal{L} \supset -m_\tau \bar{\tau}\tau + \frac{y_t}{\sqrt{2}} \bar{\tau}\left[\cos\zeta_\tau + i\gamma_5 \sin\zeta_\tau\right]\tau\, h.$$

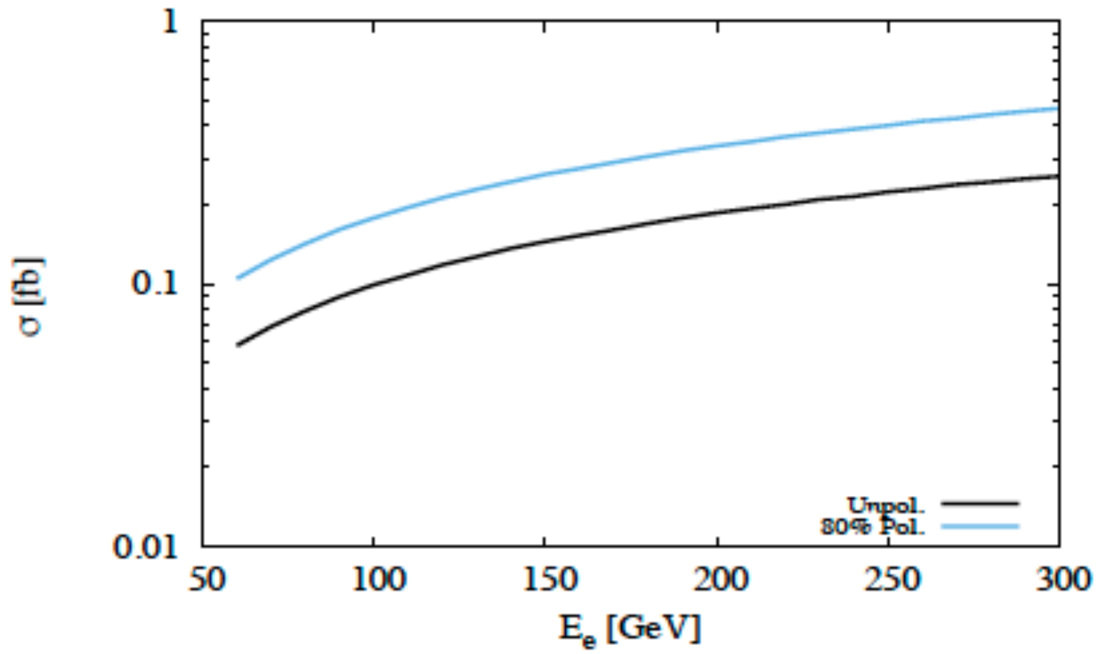

Figure 2: The total cross section against electron beam energy with and without polarization, while the proton beam energy is fixed at 7 TeV. The black solid and dotted dark black lines correspond to the process $p\, e^- \rightarrow \nu_e\, h\, j, h \rightarrow \tau^+\tau^-(\tau+ \rightarrow \pi^+\nu_\tau, \tau- \rightarrow \pi^-\bar{\nu}_\tau)$ with and without polarisation of electron beam respectively.

$$\Gamma^{\rm BSM}_{\mu\nu}(p, q) = \frac{g}{M_W}[\lambda(p \cdot q g_{\mu\nu} - p_\nu q_\mu) + i\lambda' \epsilon_{\mu\nu\rho\sigma} p^\rho q^\sigma],$$

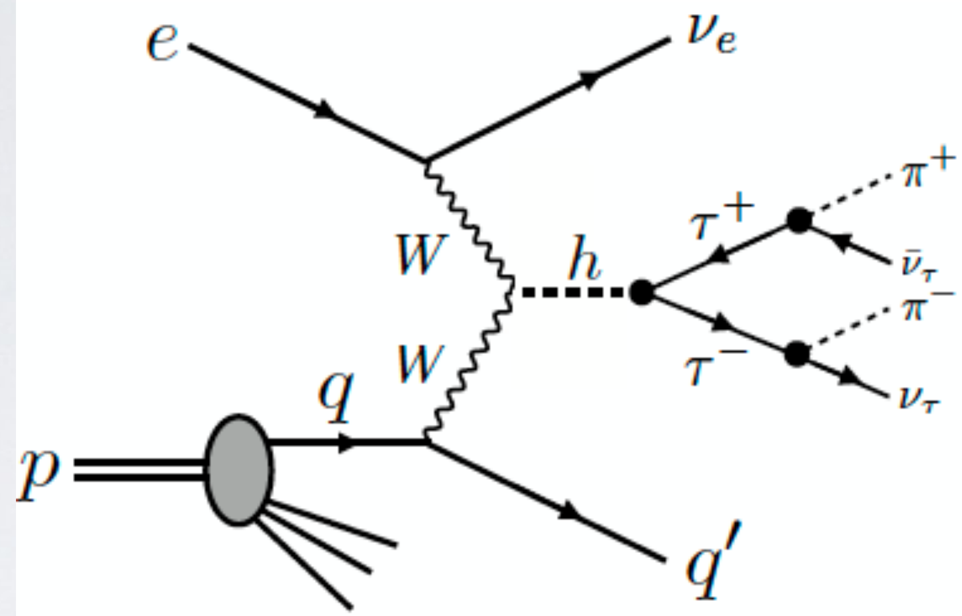

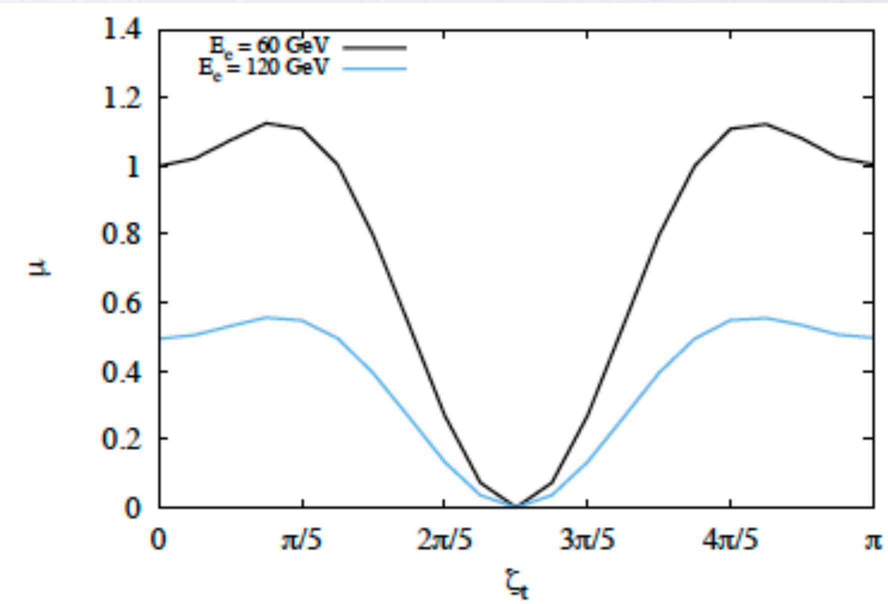

Figure 3: *The signal strength (μ) against CP phase (ζ_τ), the black solid and dotted lines correspond to the electron beam energies of 60 GeV and 120 GeV respectively, while the proton beam energy is fixed at 7 TeV.*

!!

Upcoming results

Next-to-leading order :

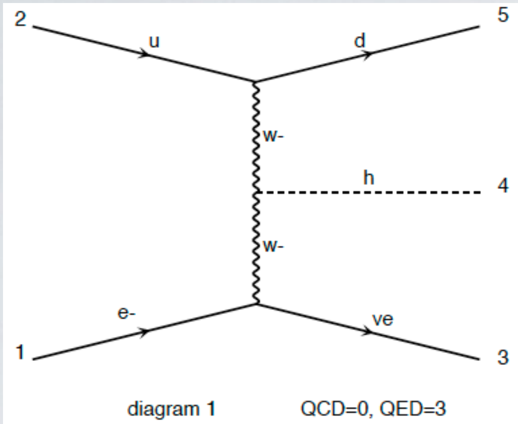

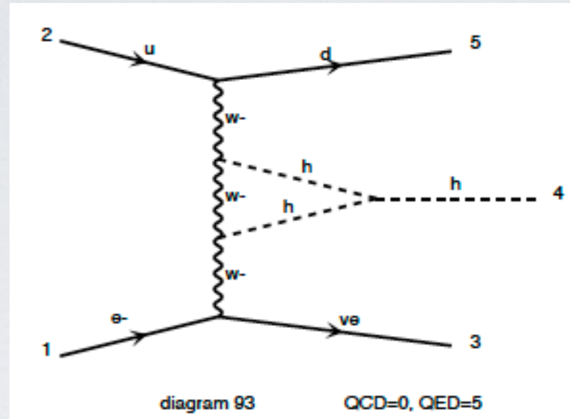

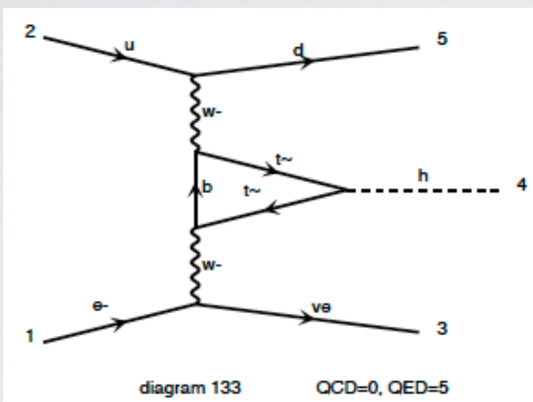

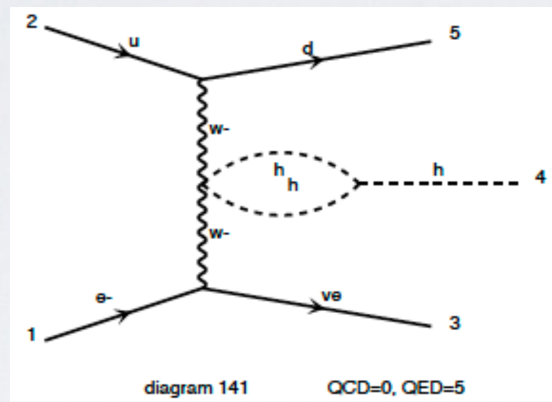

- Higher order virtual corrections in single Higgs production - interesting to measure Higgs-self couplings, WWh, WWhh, ttH couplings.
- Finite, Gauge invariant, contributions in terms of size/ numbers ?

Coupling measurements :

- Top-Yukawa at LHeC/FCC-eh
- h > tau tau
- h > bb, cc **[M. Tanaka et. al., U. Klien et.al]**
- h > WW, ZZ in fully hadronic mode, or semi-leptonic modes